The American Journal of Engineering and Technology
ISSN 2689-0984 | Open Access

TYPE Original Research
PAGE NO. 79-87
DOI 10.37547/tajet/Volume07Issue07-09

Comprehensive Analysis of Physico-Chemical and Biological Mechanisms of Reverse Osmosis Membrane Fouling with the Development and Optimization of Preventive Strategies to Enhance the Operational Stability of Membrane Systems

Andrii Odnoralov
"Technical Director", Jordan water; "Director", Fisoniya LLC Kiev, Ukraine

OPEN ACCESS
SUBMITTED 06 June 2025
ACCEPTED 24 June 2025
PUBLISHED 22 July 2025
VOLUME Vol.07 Issue 07 2025

CITATION

Andrii Odnoralov. (2025). Comprehensive Analysis of Physico-Chemical and Biological Mechanisms of Reverse Osmosis Membrane Fouling with the Development and Optimization of Preventive Strategies to Enhance the Operational Stability of Membrane Systems. The American Journal of Engineering and Technology, 7(07), 79–87. https://doi.org/10.37547/tajet/Volume07Issue07-09

Abstract: This article presents a comprehensive analysis of the physicochemical and biological mechanisms underlying reverse-osmosis membrane fouling, along with the development and optimization of preventive strategies to enhance the operational stability of membrane systems. The relevance of this research is determined by the growing freshwater scarcity and the rapid expansion of desalination capacities, where over 65% of produced water is obtained through reverse osmosis. The work aims to integrate classical and modern non-invasive fouling diagnosis methods—from SEM-EDS, ATR-FTIR, and XPS to optical coherence tomography and online ATP/BGP sensors—to delineate four primary foulant types and identify key intervention points at the early stages of deposit formation. The novelty of the study lies in the design and optimization of cascade preventive strategies that combine fine physicochemical pretreatment, targeted chemistry, and adaptive control of cleaning and reagent dosing protocols via machine-learning algorithms. The proposed closed-loop control model—from deep diagnostics to automatic adjustment of operating parameters—enables a substantial extension of the

maintenance interval and a reduction in the total cost per cubic meter of treated water. Key results demonstrate that: Inorganic fouling can be effectively suppressed by antiscalants and pH regulation, preventing irreversible carbonate and sulfate deposit formation; Organic deposits and colloidal particles are most robustly removed by combining surfactant-enhanced cleaning and membrane-surface modification with hydrophilic coatings; Biofouling is controlled through two-stage biocide protocols triggered by early signals from ATP sensors, which reduces cleaning costs and downtime to a critical minimum. Online monitoring of hydraulic and biological markers is integrated with trainable algorithms that flexibly adapt flow parameters and chemical protection in real-time. This article will appeal to specialists in membrane technology and desalination, as well as researchers and developers of reverse osmosis systems and preventive water quality management strategies.

Keywords: reverse osmosis; fouling; membrane systems; preventive strategies; optical coherence tomography; antiscalants; biofouling.

Introduction

Global growth in freshwater scarcity has compelled nations to scale up their desalination capacity rapidly. Open estimates for 2023 report approximately 18,000 plants in operation, with a combined output of nearly 100 million m^3/day, of which over 65% is produced via reverse osmosis (Ahmed et al., 2023). However, the economic efficiency of the technology remains vulnerable—membrane fouling complicates hydraulic regimes, increases required pressure, and accelerates module degradation. In full-scale systems, biofouling and associated cleanings can raise operational expenditures by 30 % or more (Sanawar et al., 2018), while energy consumption often grows faster than productivity: at one medium-size plant studied, energy costs rose by 15 % over four years, while water output increased by only 8.7 % (Feo-García et al., 2024). Given that electricity can account for up to half the cost of producing a cubic meter of water, fouling represents a key barrier to further reducing desalination costs. It is thus critically important for water security.

Modern analysis of fouling processes has evolved from post-mortem autopsies of modules to continuous non-invasive methodologies. The classical approach involves characterizing the four dominant foulant types—namely, inorganic scaling, organic and colloidal deposits, and biofilms—to inform reagent selection and cleaning protocols (Ahmed et al., 2023). SEM-EDS, ATR-FTIR, and XPS elucidate the layer morphology and chemistry, while growth dynamics are now tracked via permeability decline, transmembrane pressure rise, and signals from online ATP sensors. Special attention is devoted to optical coherence tomography. This method enables real-time visualization of deposit thickness and heterogeneity without opening spiral-wound modules, thereby significantly improving the accuracy of predictive models (Lee et al., 2023). This rich experimental foundation supports both empirical correlations and mechanistic series-resistance models, complemented by machine learning for early warning of atypical events.

The development of preventive strategies naturally follows from this diagnostic paradigm: the finer the mechanistic understanding, the earlier interventions can be applied. In practice, the most robust outcomes are achieved through a cascade combination of fine physicochemical pretreatments (microfiltration, coagulation, and controlled chlorination) with gentle biocidal or photocatalytic actions that suppress microbial activity without damaging the polyamide membrane skin (Lee et al., 2023).

These measures are supplemented by antifouling, hydrophilic self-cleaning polymer coatings, alongside adaptive flow and recovery management, to maintain shear velocity and salt-saturation levels beneath critical thresholds. It is precisely the integration of such measures—from deep diagnostics to agile regulation and considered cleaning chemistry—that delivers a real extension of module lifetime and reduction of overall water cost, making fouling prevention a central focus of ongoing research and engineering optimization in membrane systems.

Materials and Methodology

This research draws on over 20 key publications on fouling analysis in reverse-osmosis systems, encompassing both academic articles and field-scale reports. The theoretical basis comprises summaries of operational statistics for 18,000 installations with a SWRO share exceeding 65% (Ahmed et al., 2023) and assessments of biofouling impacts on costs and energy use in full-scale lines (Sanawar et al., 2018; Feo-García et al., 2024). Methodologically, emphasis is placed on integrating classical module-autopsy tools with modern non-invasive diagnostic techniques (Lee et al., 2023).

For morphological and chemical analyses of deposits, scanning electron microscopy with energy-dispersive analysis (SEM-EDS), attenuated-total-reflection Fourier-transform infrared spectroscopy (ATR-FTIR), and X-ray photoelectron spectroscopy (XPS) were employed, complemented by optical coherence tomography (OCT) for dynamic monitoring of layer thickness and heterogeneity without breaching spiral-wound modules (Lee et al., 2023). Fouling dynamics were assessed by changes in permeability, growth in transmembrane pressure, and signals from online adenosine triphosphate (ATP) and biological growth potential (BGP) sensors (Rezaei et al., 2020; Abushaban et al., 2020).

Comparative analysis of the four deposit types included laboratory tests on model foulants: inorganic scaling of $CaCO_3$ and $CaSO_4$ at varied saturation indices and temperatures (Pomerantz et al., 2006; Ashfaq et al., 2019); organic deposition of humic acids with and without nonionic surfactants (Kallapalli & Basu, 2025; Gao et al., 2023); colloidal flocculation of silica and iron oxides on unmodified and modified polyamide surfaces (Lin et al., 2021; Pipich et al., 2021); and biofouling in industrial-module autopsies, quantified as $CFU \cdot cm^{-2}$ and correlated with TMP (Kucera, 2019; Hoek et al., 2022; Vrouwenvelder et al., 2009).

The design and optimization of preventive strategies were based on pilot- and full-scale trials of cascade pretreatment—coagulation, microfiltration, and controlled chlorination—to reduce organic and colloidal fouling (Ahmed et al., 2023; Lee et al., 2023); application of phosphonates and acrylic copolymers as antiscalants (Verbeke et al., 2020; Lakner & Lakner, 2025); and biocidal protection schemes employing metabisulfite and photocatalytic complexes. For real-time control of cleaning regimes and reagent dosing, machine-learning algorithms were implemented to analyze flow data, pressure differentials, and salt passage, automatically adjusting process parameters (Roth et al., 2024).

Results and Discussion

The physicochemical picture of fouling in reverse-osmosis modules can be reduced to four archetypes, each distinguished by its dominant nucleation mechanism, typical nutrient sources in the stream, and characteristic permeability loss. Inorganic fouling—primarily carbonate and sulfate scaling—begins when the local supersaturation rises faster than hydrodynamic shear dispersion can mitigate. Autopsies of industrial SWRO modules treated only by ultrafiltration showed that calcium deposits comprise up to 77.5 % of the foulant layer's mass; the addition of an adsorptive pre-treatment halved this proportion while simultaneously reducing transmembrane-pressure (ΔP) increase by 10–30 % (Wang et al., 2022).

Retained salts crystallize as calcite, aragonite, or gypsum and, under extreme concentrate-recovery ratios, can collapse permeate flux to half its initial value (Rezaei et al., 2020). Manufacturers, therefore, recommend initiating acid cleaning once ΔP has risen by 15% to prevent the transition into an irreversible stone-crust stage (Lakner & Lakner, 2025).

Organic fouling is generated by humic acids, surfactants, and low-molecular-weight polar compounds that adsorb onto the hydrophobic domains of polyamide and penetrate pores via hydrogen bonding and π–π interactions. In a laboratory test, humic acid alone yielded 57 % irreversibly bound carbon after a standard hydraulic rinse. In contrast, the inclusion of nonionic surfactants reduced that fraction to 20 % and maintained operating pressure between 83 and 105 kPa (Kallapalli & Basu, 2025). A combined humic-protein-alginate mixture at only 50 mg/L lowered flux by 21.7 %, and in the presence of 0.5 mM Mn^{2+} accelerated permeability decline to 66.8 % due to the formation of dense organo-mineral co-aggregates, as shown in Figure 1 (Gao et al., 2023).

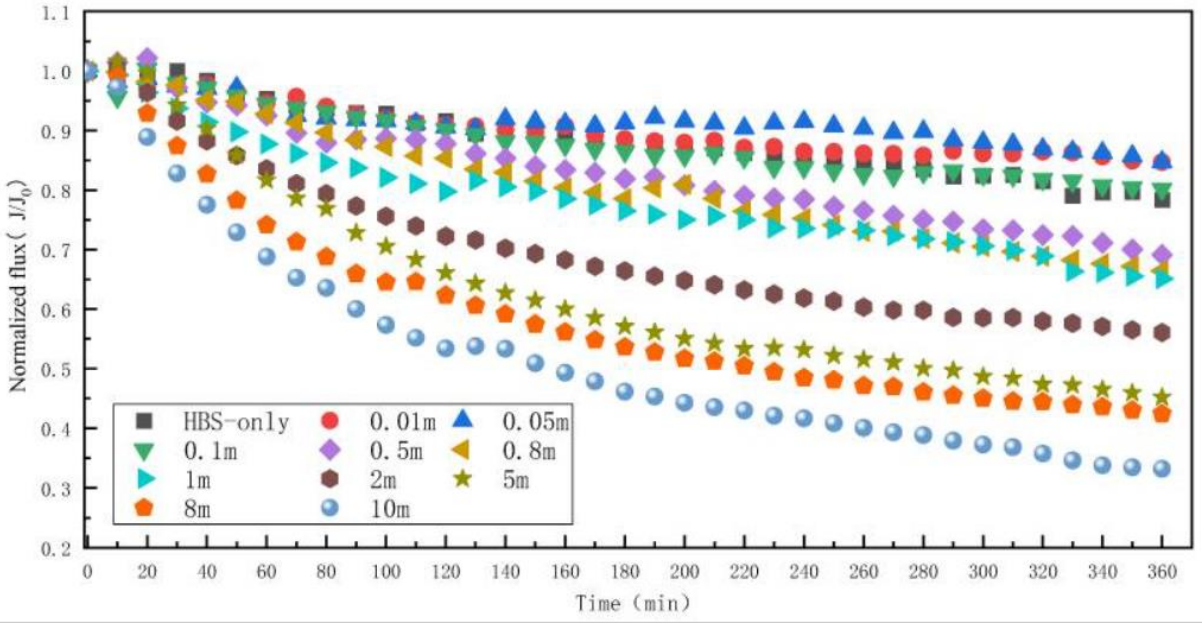

Fig. 1. Effect of different Mn2+ concentrations on RO membrane fouling caused by HBS (Gao et al., 2023)

This effect is most pronounced at neutral pH and high Ca^{2+} concentration since these ions are complex with NOM oxygen groups, promoting layer compaction.

Biofouling begins with the colonization of the adsorbed organic film, leading to the exponential growth of an exopolysaccharide matrix that obstructs feed channels and impairs shear cleaning. Global expenditures for the prevention and remediation of biofouling in desalination are estimated to be approximately $ 15 billion per year. Industrial lines reach the cleaning threshold, and TMP increases within 6–10 weeks, underscoring the relative inexpensiveness of timely prevention versus downtime (Ahmed et al., 2023). According to DuPont FilmTec guidelines, cleaning should be initiated at a 15 % increase in hydraulic gradient, lest the biofilm progress to a dense, mineralized crust that is poorly soluble at elevated pH (Lakner & Lakner, 2025).

Colloidal fouling is formed by silicates, iron-oxide flocs, and organo-clay particles ranging from 100 nm to several micrometers. Their deposition intensifies when the polyamide surface charge is partially screened by divalent cations, resulting in reduced dispersion due to coagulation. On unmodified membranes, a layer of amorphous silica reduced flux by 53% and left less than 1% reversible fouling after rinsing; modification with cationic monomers reduced the irreversible fraction to 13–33%, highlighting the key role of electrostatic forces in colloidal cake formation (Lin et al., 2021). Although colloids generally do not chemically interact with polyamide, they form a diffusion barrier and provide a scaffold for subsequent biofilm and crystal growth, making their early removal an essential element of comprehensive protection.

Thus, each foulant group has its primary driver: supersaturation for inorganics, hydrophobic and ionic interactions for organics, microbial metabolism for biofouling, and colloidal destabilization for solid-dispersed particles. Despite their differing natures, these mechanisms reinforce one another, forming a hierarchical deposit layer. Effective prevention, therefore, requires precise identification of the prevailing foulant type and deployment of targeted measures before the TMP increase exceeds the operational threshold. The classification above establishes the analytical framework for subsequent sections, which will examine detailed nucleation mechanisms, growth kinetics, and optimal suppression strategies for each fouling type.

The active polyamide-skin surface layer is the primary reactive center, and any chemical attack rapidly translates into performance loss. Among the most aggressive factors is active chlorine: 50 ppm NaOCl at pH 4 for just 2.5 hours reduced water permeability by approximately 40% due to hydrogen-bond cleavage and amide-group chlorination, whereas alkaline treatment produced only moderate compaction and a slight increase in selectivity (Verbeke et al., 2020). In addition to oxidants, Fe^{2+}/Cu^{2+} ions catalyze the radical-driven crosslinking and hydrolysis of polyamide, and the sorption of surfactant organics increases hydrophobicity, facilitating subsequent inorganic deposition.

Acid-base conditions fundamentally alter the charge

architecture of the active layer. At pH ≈ 3–4, carboxyl groups are largely undissociated, and the ζ-potential is near zero; at pH 8–9, it shifts to ≤ –10 mV, enhancing electrostatic repulsion of colloids and macro-ions (Pipich et al., 2021). A comprehensive study showed that the addition of sticky monocations ($Cs^+ > Na^+ > Li^+$) or polarizable Cl^- ions could partially screen or even invert the negative surface charge, directly affecting ion permeation and water flux (Roth et al., 2024), as illustrated in Figure 2.

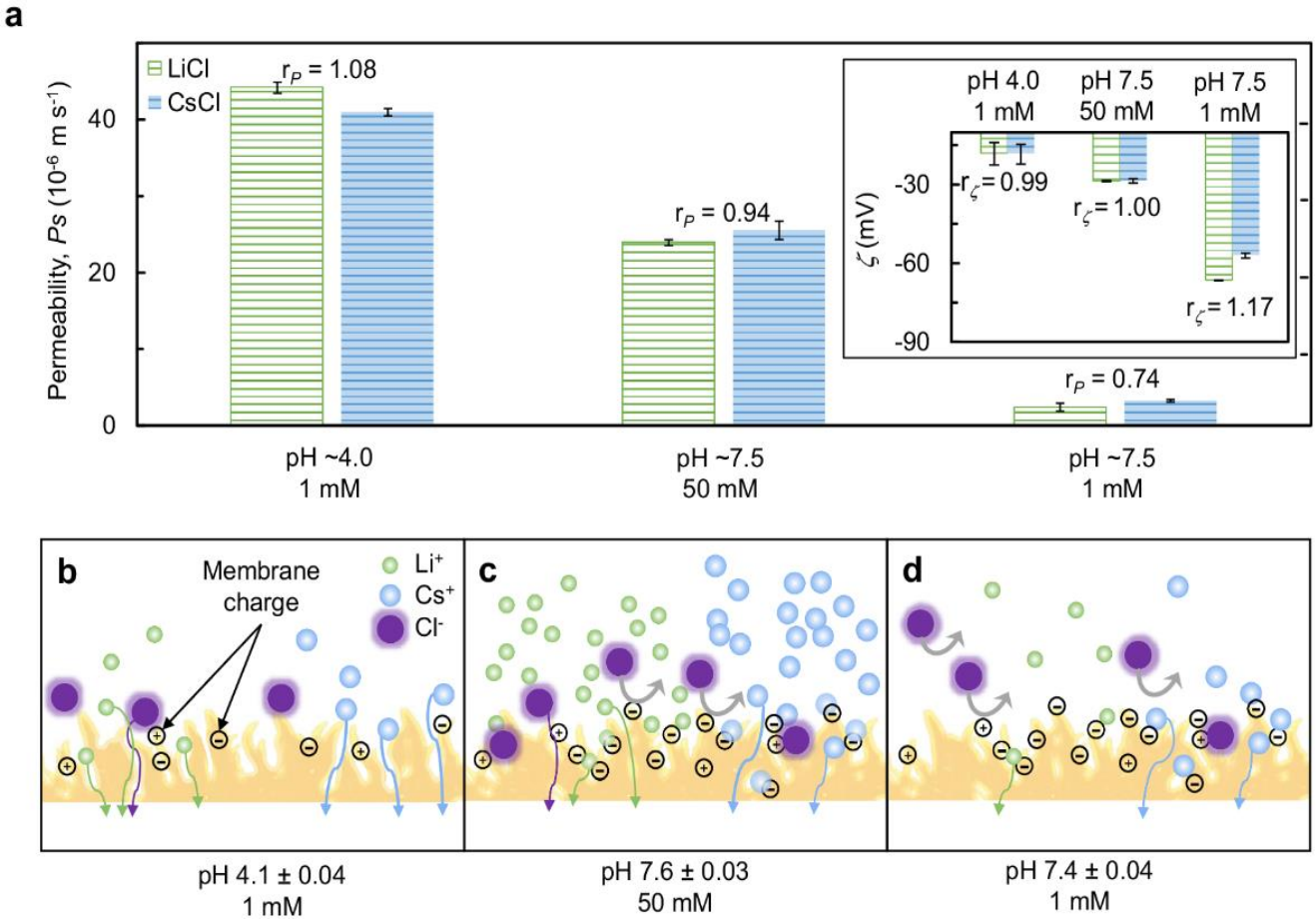

Fig. 2. Correlation between membrane zeta potential and ion permeability (Roth et al., 2024)

Divalent Ca^{2+} and Mg^{2+} ions form ionic bridges between carboxyl groups and promote the layering of organic acids and humic substances, thereby preparing the substrate for a mixed organo-mineral cake. Temperature simultaneously accelerates diffusion and increases the rate constants of crystallization. Under high cross-flow, this amplifies the concentration gradient in the boundary layer. In an industrial cell, this is equivalent to an increase in local salinity at the membrane surface relative to the bulk, which directly raises the osmotic pressure and consumes net driving pressure, accelerating the transition from concentration polarization to actual salt scaling.

When the surface concentration reaches the product-critical threshold, nucleation processes commence. For $CaSO_4$ at a saturation index up to 3.0, the induction period in a continuously stirred solution was 150–270 min; periodic flow reversal was sufficient to reset the induction time and completely suppress precipitation for up to 8 h (Pomerantz et al., 2006). Once crystallization begins, permeability declines in an avalanche-like manner: laboratory tests revealed that flux-versus-time curves at varying Reynolds numbers and temperatures converge toward a critical flux. Increasing temperature accelerates the growth of acicular gypsum crystals, thereby increasing hydrodynamic resistance and deposit mass ($R^2 \geq 0.97$ between deposit mass and T) (Ashfaq et al., 2019). Under pH-dependent reductions in carbonate solubility, a similar pattern emerges at even lower saturation indices—local pH rises due to CO_2 degassing in the outer, dehydrated layers are sufficient to trigger scale formation.

Thus, chemical modifications of the active layer, changes in its charge, and surface energy induced by pH and ionic composition, together with kinetic effects of temperature and concentration polarization, mutually reinforce one another and set the initial conditions for crystallization.

The bacterial load in feedwater is rarely sterile. Analysis of 150 autopsied industrial modules revealed that at just 10,000 CFU·cm^{-2} on the membrane surface, the system enters the problematic category according to biofouling indicators. A concentration of 1000 CFU·mL^{-1} in the concentrate reliably correlates with an accelerated rise in transmembrane pressure (Kucera, 2019). For rapid online control, bacterial growth potential via ATP is increasingly employed: at a full-scale SWRO plant, raising the BGP in the feed from 100 to 950 µg C·L^{-1} led to a monotonic increase in normalized ΔP and a parallel decrease in permeability over three months of operation, confirming the metric's predictive value (Abushaban et al., 2020). Such biological nutrient load of the feed stream determines the initial colonization of the fresh polyamide surface, whose properties by that time have already been altered by the pH- and ion-induced charge shifts described above.

The first stage of biofilm formation involves the conditioning of an organic film, a coating a few nanometers thick, which neutralizes the membrane's native hydrophilicity and provides sites for the reversible electrostatic adsorption of bacteria. Modeling aligned with nutrient-profile data indicates that, given an easily assimilable substrate, biofilm thickness near the inlet of an element reaches ≈ 200 µm by day 20. In contrast, at the outlet, it remains around 1 µm—this gradient reflects nutrient depletion along the channel, as illustrated in Figure 3 (Hoek et al., 2022).

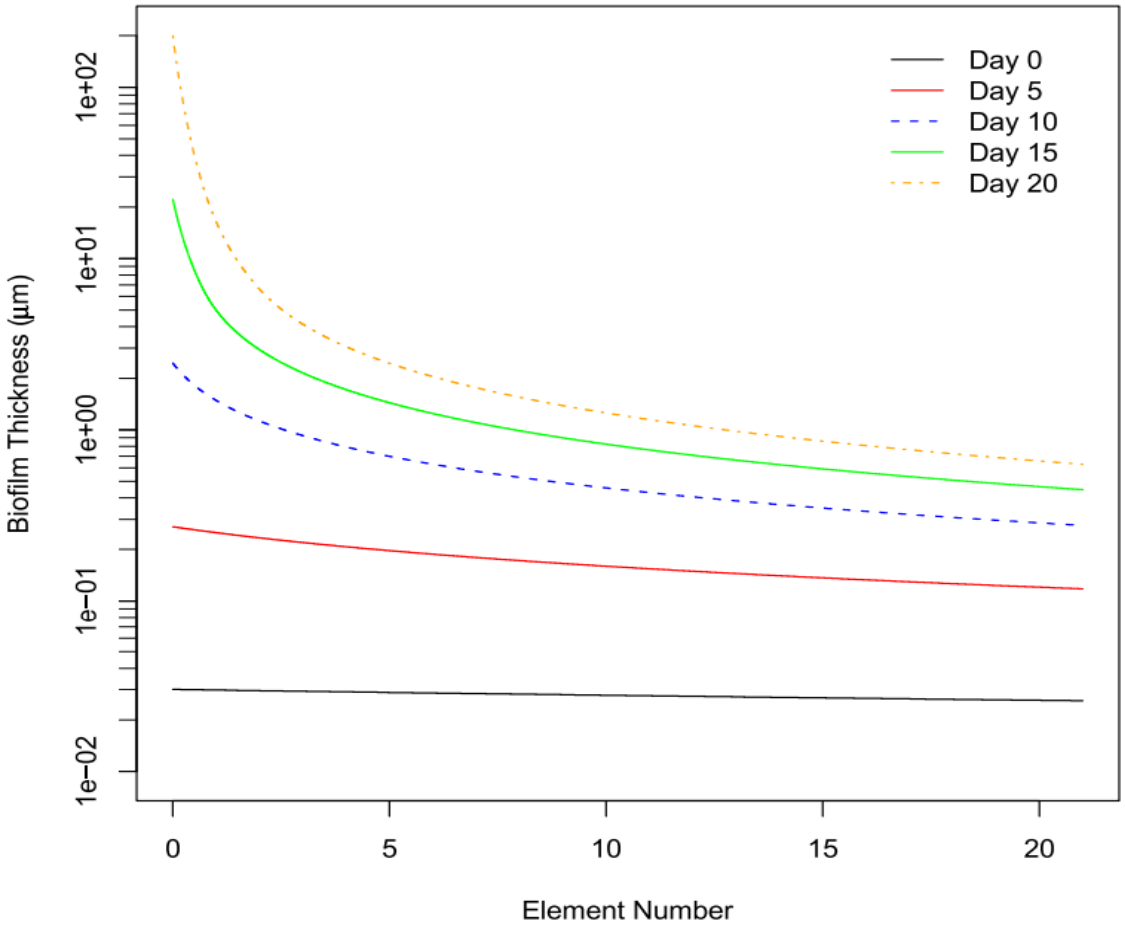

Fig. 3. Model illustration of local substrate-limited biofilm growth kinetics and biofilm thickness (Hoek et al., 2022)

Exponential growth is accompanied by the incorporation of Ca^{2+} and Mg^{2+} into the EPS matrix, creating a porous micro-reactor within which pH and ionic strength deviate from bulk values, further promoting local scaling and cementation of the biofilm.

A direct consequence of these processes is increased hydraulic resistance. In membrane simulators, increasing the load by 100–400 µg C/L (as acetate equivalent) accelerated biomass accumulation. It caused ΔP to grow by 0.2 bar over 7 days, whereas lowering the substrate load slowed the trend and allowed reversible ΔP reduction by merely decreasing the cross-flow velocity (Vrouwenvelder et al., 2009). Biofilm accumulation also alters flow distribution. Computational analysis has shown a shift in the peak flux from leading elements toward the tail due to a decline in inlet TMP and the forced redistribution of load, which

induces additional internal polarization (Hoek et al., 2022). Beyond purely hydraulic losses, microbial metabolic activity affects selectivity: acidic and amylolytic enzymes, as well as free chlorine generated within the biofilm, can increase water permeability by up to 70 % while simultaneously linearly reducing salt rejection, indicating degradation of the polyamide matrix (Kucera, 2019).

Thus, biofouling unites the trigger aspects of chemistry and hydrodynamics—nutrient micro-pulses, electrostatic screening, and concentration polarization—forming a self-sustaining layer that not only physically blocks channels but chemically ages the active composite. It is precisely at this intersection that the key intervention points lie, and these are discussed further in the section on preventive strategies.

The reliable operation of RO trains begins with precise monitoring of primary fouling markers. Spiral-wound module manufacturers recommend initiating cleaning as soon as the normalized ΔP increases noticeably, the permeate flux drops measurably, or the salt passage rises relative to the startup values. These three parameters—a module pressure drop, normalized flux, and salt passage—remain the foundation of daily monitoring, as they can be temperature-corrected and restored to baseline after cleaning, thereby objectively assessing membrane fatigue and the effectiveness of the cleaning process.

Hydraulic indicators detect an already established layer, whereas biological signals respond earlier. Flow cytometry and ATP sensors detect viable-cell growth long before a notable ΔP rise, and a monotonic increase in permeate bacterial potential reliably predicts subsequent growth in channel resistance. Such early warning affords the operator time for rapid disinfection or antifoulant-dosing adjustment, preventing unplanned shutdowns.

When membranes are finally opened, a vast arsenal of autopsy techniques is applied. SEM-EDS locates crystallization centers even within multilayer organo-mineral crusts, while infrared spectroscopy distinguishes humates and polysaccharides in the biofilm. Combined with confocal tomography, these methods yield a three-dimensional map of layer thickness and porosity, serving as the basis for validating hydrodynamic polarization models.

Diagnostic data forms the architecture of prevention. The first barrier is deep pretreatment, which involves coagulation with iron or aluminum salts to aggregate particles, shift their charge into the near-neutral range, and markedly reduce the ΔP rise compared to cartridge filtration alone. When combined with ultrafiltration, only traces of colloids larger than the micron range remain in the feed, significantly reducing the likelihood of early colloidal-cake formation and delivering energy savings through lower operating pressure.

For the control of inorganic scaling, antiscalants—phosphonates and acrylic copolymers—play a key role by suppressing gypsum and calcite nucleation across operating saturation-index ranges. In contrast, optimized dosing control extends the cleaning interval several-fold. Concurrent mild acidification reduces carbonate-ion activity, further decreasing crystallization rates and lowering inhibitor consumption without compromising recovery.

Biofouling is countered in two stages: first, by dechlorination with excess metabisulfite, and then by periodic pulses of a non-oxidizing biocide. This scheme maintains ΔP within the operating corridor and permits significantly longer intervals between complete clean-in-place cycles than standard schedules.

The growth of operational data volume has enabled automated regime optimization. Deep-learning algorithms, trained on flux, pressure drop, and salt passage variations, already demonstrate the ability to select feed pressure and recovery to sustain near-complete salt rejection at minimal energy consumption, while simultaneously postponing CIP dates. When coupled with digital biological-activity sensors, these controllers transform diagnostics into a closed-loop control system in which any detected anomaly automatically triggers adjustments to flow, pH, or chemical dosing.

The synergy of real-time indicators, advanced analytics, and adaptive control underpins the longevity of membrane systems. The earlier a deviation is detected—whether a jump in ΔP, a spike in biological activity, or a change in spectral signature—the gentler and cheaper the corrective action. By unifying fine pretreatment, targeted reagents, biological monitoring, and machine optimization into a single cycle, operators achieve stable permeability and a predictable cost per cubic meter of produced water—the ultimate goal of a fouling-prevention strategy.

Thus, the comprehensive analysis of reverse-osmosis fouling mechanisms demonstrates that the key to

stable, economical membrane operation lies in sequential implementation of integrated preventive measures: from deep pretreatment and pinpoint chemical protection to online monitoring of hydraulic and biological markers, followed by adaptive control of wash cycles and reagent dosing. Only by accounting for the interdependence of carbonate, organic, colloidal, and biological fouling—as well as the influence of pH, ionic composition, and temperature—can the operating strategy be adjusted in time to minimize irreversible deposits and extend maintenance intervals. This holistic combination of diagnostics, targeted chemistry, and intelligent control lays a robust foundation for further development of membrane systems. It guides the final recommendations for optimizing and enhancing the cleaning process and improving water security.

Conclusion

The comprehensive analysis of physicochemical and biological fouling mechanisms in reverse-osmosis membranes has revealed that the primary drivers of deposit formation and development are local supersaturation of salt components, hydrophobic and ionic interactions of organic substances, microbial metabolic activity, and colloidal instability. Each foulant type—carbonate and sulfate scaling, organic fouling, biofilm formation, and colloidal cake—contributes to hydraulic-regime degradation, including reduced permeability, increased transmembrane pressure, and accelerated deterioration of the polyamide active surface. Moreover, interactions among foulant groups amplify one another, creating a hierarchical, hard-to-remove cake, which necessitates early diagnosis of the predominant foulant type before TMP reaches critical levels or permeate flux declines significantly.

Modern fouling-diagnosis methods, including SEM-EDS, ATR-FTIR, XPS, and especially optical coherence tomography, enable real-time tracking of deposit thickness and morphology without module disassembly. Combining these tools with online sensors for pressure drop, normalized flux, and biological markers (ATP analysis, BGP) generates the rich experimental database required for both empirical correlations and the development of mechanistic models and machine--learning algorithms. This approach provides early warning of abnormal events and enables rapid adjustment of operating parameters, thereby markedly improving forecast accuracy and the efficacy of preventive interventions.

The practical implementation of preventive strategies is built upon the integration of deep pretreatment (coagulation, microfiltration, and controlled chloramination), targeted chemical reagents (phosphonates, acrylic copolymers, non-oxidizing biocides, and photocatalysts), and adaptive control of cleaning and flow regimes. A cascade combination of fine physicochemical feed preparation with gentle biocidal measures suppresses organic and biological fouling without damaging the polyamide layer. Antifouling surface coatings and shear-rate management, combined with deep-learning algorithms for automatic adjustment of pressure, reagent doses, and recovery, create a closed control loop that unites diagnostics, response, and real-time performance analysis.

Consequently, a systematic approach—from precise identification of the dominant foulant type to adaptive control and intelligent optimization—emerges as the key factor in extending membrane life and reducing the cost per cubic meter of produced water. The sequential integration of diagnostic technologies, targeted cleaning chemistry, and machine--driven operation control ensures stable permeability, predictable operating expenses, and minimization of irreversible deposits. Such a comprehensive suite of measures provides a solid foundation for future engineering optimizations of membrane systems and enhanced water security.

References

1. Abushaban, A., Salinas-Rodriguez, S. G., Kapala, M., Pastorelli, D., Schippers, J. C., Mondal, S., Goueli, S., & Kennedy, M. D. (2020). Monitoring Biofouling Potential Using ATP-Based Bacterial Growth Potential in SWRO Pre-Treatment of a Full-Scale Plant. *Membranes*, *10*(11), 360–360. https://doi.org/10.3390/membranes10110360
2. Ahmed, M. A., Amin, S., & Mohamed, A. A. (2023). Fouling in Reverse Osmosis membranes: monitoring, characterization, Mitigation Strategies and Future Directions. *Heliyon*, *9*(4), e14908. https://doi.org/10.1016/j.heliyon.2023.e14908
3. Ashfaq, M. Y., Al-Ghouti, M. A., & Da'na, D. A. (2019). Investigating the effect of temperature on calcium sulfate scaling of reverse osmosis membranes using FTIR, SEM-EDX, and multivariate analysis. *The Science of the Total Environment*, *703*, 134726–134726. https://doi.org/10.1016/j.scitotenv.2019.134726

4. Feo-García, J., Pulido-Alonso, A., Florido-Betancor, A., & Florido-Suárez, N. R. (2024). Cost Studies of Reverse Osmosis Desalination Plants in the Range of 23,000–33,000 m3/day. *Water*, *16*(6), 910. https://doi.org/10.3390/w16060910

5. Gao, Q., Duan, L., Jia, Y., Zhang, H., Liu, J., & Yang, W. (2023). Differences in the Effect of Mn2+ on the Reverse Osmosis Membrane Fouling Caused by Different Types of Organic Matter: Experimental and Density Functional Theory Evidence. *Membranes*, *13*(10), 823–823. https://doi.org/10.3390/membranes13100823

6. Hoek, E. M. V., Weigand, T. M., & Edalat, A. (2022). Reverse osmosis membrane biofouling: causes, consequences, and countermeasures. *Npj Clean Water*, *5*(1). https://doi.org/10.1038/s41545-022-00183-0

7. Kallapalli, N., & Basu, O. D. (2025). Surfactant-Enhanced Cleaning Solutions for Ceramic Membranes: A Comparative Study on Humic Acid and BSA Fouling. *Membranes*, *15*(3), 73–73. https://doi.org/10.3390/membranes15030073

8. Kucera, J. (2019). Biofouling of Polyamide Membranes: Fouling Mechanisms, Current Mitigation and Cleaning Strategies, and Future Prospects. *Membranes*, *9*(9), 111. https://doi.org/10.3390/membranes9090111

9. Lakner, J., & Lakner, G. (2025). Prediction of Expected Fouling Time During Transmembrane Transition in Reverse Osmosis Systems. *Membranes*, *15*(6), 170–170. https://doi.org/10.3390/membranes15060170

10. Lee, S., Cho, H., Choi, Y., & Lee, S. (2023). Application of Optical Coherence Tomography (OCT) to Analyze Membrane Fouling under Intermittent Operation. *Membranes*, *13*(4), 392–392. https://doi.org/10.3390/membranes13040392

11. Lin, Y.-L., Zheng, N.-Y., Gan, H.-Y., Chang, A.-X., Luo, H.-X., & Mao, Y.-J. (2021). Mitigating Silica Fouling and Improving PPCP Removal by Modified NF90 Using In Situ Radical Graft Polymerization. *Membranes*, *11*(11), 904. https://doi.org/10.3390/membranes11110904

12. Pipich, V., Starc, T., Buitenhuis, J., Kasher, R., Petry, W., Oren, Y., & Schwahn, D. (2021). Silica Fouling in Reverse Osmosis Systems–Operando Small-Angle Neutron Scattering Studies. *Membranes*, *11*(6), 413–413. https://doi.org/10.3390/membranes11060413

13. Pomerantz, N., Ladizhansky, Y., Korin, E., Waisman, M., Daltrophe, N., & Gilron, J. (2006). Prevention of Scaling of Reverse Osmosis Membranes by Zeroing the Elapsed Nucleation Time. Part I. Calcium Sulfate. *Industrial & Engineering Chemistry Research*, *45*(6), 2008–2016. https://doi.org/10.1021/ie051040k

14. Rezaei, M., Alsaati, A., Warsinger, D. M., Hell, F., & Samhaber, W. M. (2020). Long-Running Comparison of Feed-Water Scaling in Membrane Distillation. *Membranes*, *10*(8), 173–173. https://doi.org/10.3390/membranes10080173

15. Roth, R. S., Birnhack, L., Avidar, M., Hjelvik, E. A., & Straub, A. P. (2024). Effect of Solution Ions on the Charge and Performance of Nanofiltration Membranes. *Npj Clean Water*, *7*(1). https://doi.org/10.1038/s41545-024-00322-9

16. Sanawar, H., Pinel, I., Farhat, N., Kruithof, J. C., & Vrouwenvelder, J. S. (2018). Enhanced biofilm solubilization by urea in reverse osmosis membrane systems. *Water Res X*, *1*, 100004–100004. https://doi.org/10.1016/j.wroa.2018.10.001

17. Verbeke, R., Eyley, S., Szymczyk, A., Thielemans, W., & Vankelecom, I. F. J. (2020). Controlled chlorination of polyamide reverse osmosis membranes at real scale for enhanced desalination performance. *Journal of Membrane Science*, *611*, 118400. https://doi.org/10.1016/j.memsci.2020.118400

18. Vrouwenvelder, J. S., Hinrichs, C., Van der Meer, W. G. J., Van Loosdrecht, M. C. M., & Kruithof, J. C. (2009). Pressure drop increase by biofilm accumulation in spiral wound RO and NF membrane systems: role of substrate concentration, flow velocity, substrate load, and flow direction. *Biofouling*, *25*(6), 543–555. https://doi.org/10.1080/08927010902972225

19. Wang, J., Sim, L. N., Ho, J. S., Nakano, K., Kinoshita, Y., Sekiguchi, K., & Chong, T. H. (2022). Evaluation of Ceramics Adsorption Filter as a Pretreatment for Seawater Reverse-Osmosis Desalination. *Membranes*, *12*(12), 1209. https://doi.org/10.3390/membranes12121209